Consensus-based Cooperative Formation Guidance Strategy for Multi-parafoil Airdrop Systems

Qi Chen, Yuxiang Sun, *Member, IEEE*, Min Zhao, Ming Liu, *Senior Member, IEEE*

***Abstract*— Parafoil airdrop is an important way to deliver goods and materials to area where road vehicles are not easy to reach. However, it is difficult to deliver large quantities of goods and materials to a given location with only one parafoil. Airdropping multiple parafoils is an effective choice for transporting large quantities of goods and materials. In order to realize the cooperative airdrop of multiple parafoils, a cooperative guidance framework is proposed. First, a trajectory planning algorithm is designed to plan the multiphase trajectory for the parafoil group. Then, a trajectory tracking algorithm is developed for the pilot parafoil in the parafoil group to reliably follow the planned trajectory. Finally, a cooperative formation guidance strategy is designed based on the leader-follower consensus theory. Under this strategy, the position and speed of the follower parafoil can consensus with that of the leader parafoil. Lyapunov's theorem proves the stability of this strategy. We evaluate the effectiveness of this framework through simulations. The results demonstrate that our algorithms can realize the precise airdrop of massive goods and materials with upwind landing using multiple parafoils. In addition, the parafoils could be gradually gathered to a desired formation and safe distances could be maintained between parafoils during the airdrop process.**

***Note to Practitioners*—This paper was motivated by the problem of airdropping massive goods and materials. Existing methods usually adopt a single heavy parafoil, or use centralized multi-parafoil systems. Both these methods have their limitations. For the former, there is an upper limit of the load capacity for a single parafoil. For the latter, the parafoils in the centralized system lack fully autonomous ability. Distributed multi-parafoil systems could solve the problem effectively. However, compared to single-parafoil systems, there are still some challenges; for example, the multi-parafoil gathering, collision avoidance and cooperative formation, as well as the upwind landing. Fortunately, existing parafoils are equipped with sensors, communication and control devices, so they could be viewed as agents with autonomous capabilities. In this paper, a formation guidance framework for multiple autonomous parafoils is proposed. Firstly, we plan a trajectory for the pilot parafoil. Then, we show how to effectively track the planned trajectory. Finally, we demonstrate how multiple parafoils could coordinate with each other to accomplish airdrop tasks. The simulation results confirm the feasibility of this strategy.**

This work was supported in part by the Natural Science Foundation of China under Grant No. 51875289 and No. 61873124, the Aeronautical Science Foundation of China under Grant No. 2016ZD52036, Jiangsu Province Youth Funding under Grant No. BK20150746, Jiangsu Innovation Program for Graduate Education under Grant No. KYLX15_0271. *(Corresponding author: Min Zhao)*

Qi Chen and Min Zhao are with College of Automation Engineering, Nanjing University of Aeronautics and Astronautics, 210016, China. Qi Chen is also with Faculty of Electronic Information Engineering, Huaiyin Institute of Technology, Huaian, 223003, China (email: chenqi2070@126.com; xymzhao@126.com).

Yuxiang Sun and Ming Liu are with the Department of Electronic and Computer Engineering, Hong Kong University of Science and Technology, Clear Water Bay, Kowloon, Hong Kong SAR, China (email: sun.yuxiang@outlook.com, eeyxsun@ust.hk; eelium@ust.hk).

***Index Terms*—Multi-parafoil Systems, Multi-agent Systems, Trajectory Planning, Tracking, Consensus, Formation Control**

I. Introduction

Parafoil is a kind of precise airdrop device with high lift-to-drag ratio and good manoeuvrability. It can deliver goods and materials to a designated place quickly, and expand the traditional ground transportation to 3-D space. Parafoil airdrop can be used in various applications, such as earthquake relief, military material transport, aircraft recovery, etc. During earthquakes, for example, a large amount of drugs, foods and drinking water can be airdropped to victims. In battlefields, many weapons and ammunitions can be delivered to ground forces via airdropping. Currently, researchers in the field of parafoil airdrops are mainly focusing on single-parafoil systems, for instance, the analysis of aerodynamic characteristics [1]–[3], system modelling [4]–[6], trajectory planning [7]–[9] and trajectory tracking [10]–[13] for single-parafoil systems. However, it is usually difficult to quickly deliver a massive amount of goods and materials to designated place with only one parafoil, so it is of great practical and theoretical value to study the coordinated airdrop of multiple parafoils.

There are two main solutions to airdrop massive goods and materials. One solution is to use a heavy single-parafoil system, which can carry heavy loads. Several large heavy single-parafoil systems have been developed, such as the European Space Agency's FASTWing guidance parafoil [14] and NASA's X-38 guidance parafoil [15], which have a carrying capacity of 6 tons and 11.3 tons, respectively. However, a larger parafoil requires a larger plane to accommodate the system, so there exists an upper limit of carrying capacity for a heavy single-parafoil system. In addition, the cost of a heavy single-parafoil system is high. Moreover, if the parafoil is damaged, the whole airdrop mission may fail.

Another solution is to use a multi-parafoil system, which consists of multiple medium-sized parafoils. Fig. 1 shows a schematic view of a multi-parafoil systems. The multiple parafoils are dropped at the same time, and then fly in coordination with each other to the target point without collision. Multi-parafoil airdrop systems are of great strategic significance and have raised increasing attention. The U.S. department of defence has proposed a prototype of multi-parafoil systems called the MDS3, which is part of the Joint Precision Airdrop System (JPADS) [16] and allows massive goods and materials to be delivered to the designated place via multiple JPADS parafoils.

Coordinated control of multiple parafoils is an important problem needing to be considered during the airdrop process.

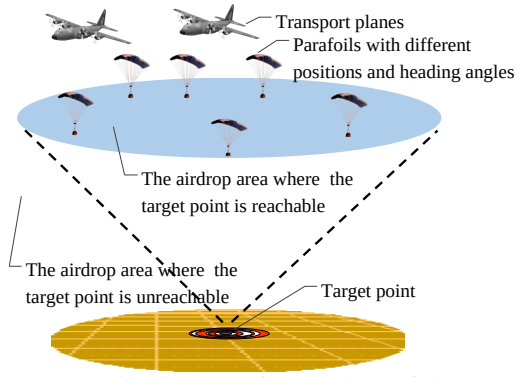

Fig. 1: Schematic diagram of a multi-parafoil system. Multiple parafoils are released at the same time. The parafoils in the cone area have sufficient height to move to the target point. In this paper, we assume that the initial position of each air-dropped parafoil lies within the cone area.

Calise *et al.* [17] pointed out that multiple parafoils deployed in the same airspace should fly in formation, so as to minimize the possibility of collisions and make the individual parafoils arrive at the target site in an organized manner. Kaminer *et al.* [18] pointed out that the use of multiple high glide parafoil systems allows for more coordinated payload delivery. In the case of deploying a military unit to a compact area, multi-parafoil systems can deliver the payload in the certain battle formation, which allows the force to operate immediately after landing without delay in regrouping.

In recent years, formation motion of many autonomous systems has been well studied, such as formation control of multi-robot systems [19], [20], formation flight of multi-UAV systems [21], coordinated control of multiple surface and underwater vehicles [22], [23], etc. However, these studies have mainly focused on how to form a formation, yet formation is only one aspect of realizing coordinated airdrop for multi-parafoil systems. How to make the formation accurately track the planned trajectory and then land in the target area is more important. Multi-parafoil systems do not work with the scenarios described in the above literature. First, parafoils dropped from different initial positions and headings need to gradually gather together during the airdrop process, rather than scattering apart, or drifting into unfriendly territory or unreachable areas, which could make the airdropped goods and materials difficult to gather. Second, the parafoils need to be kept at a safe distance from each other, otherwise they may collide with each other and fail the delivery mission.

In this paper, we propose a novel cooperative guidance airdrop framework. To the best of our knowledge, this is the first work that uses a consensus-based cooperative airdrop method for distributed multi-parafoil systems. Compared with centralized systems [24], systems with our strategy could be more flexible. The main contributions of the paper are summarized as follows:

1) We propose a cooperative formation guidance framework for large-scale airdrops, which integrates a multiphase trajectory planning algorithm and a trajectory tracking algorithm. The planned trajectory is easy to be realized in practice with simple operations. The new trajectory tracking algorithm that combines lateral and longitudinal tracking control for the pilot parafoil is able to reliably track the planned trajectory.
2) We develop a formation guidance strategy for multi-parafoil systems, which introduce a collision avoidance term to ensure that all parafoils form a collision-free formation, track the planned trajectory and eventually land upwind to a designated point.

The simulation results show that the parafoils are able to land on designated points precisely, and do not scatter everywhere. Moreover, the strategy does not require all the follower parafoils to communicate with the pilot parafoil, and the followers can realize cooperative formation just through local communications with neighbourhoods, which reduces the risk of electromagnetic exposure during communications. In addition, since only the pilot parafoil needs to be equipped with the device for receiving the planned trajectory information, the other followers do not need such equipment, so the cost can be reduced.

The remainder of this paper is structured as follows. In Section II, related works are reviewed. In Section III, the preliminaries are introduced. In Section IV, we present the details of the algorithms. In Section V, experimental results and discussions are presented. Conclusions and future work are drawn in the last section.

II. Related Work

Research on multi-parafoil airdrops is quite limited. Luo *et al.* [24] proposed a trajectory planning and gathering strategy for multi-parafoil systems based on the pseudo-spectral method. The problem of trajectory planning for multi-parafoil systems was transformed into an optimal control problem with a set of nonlinear and complex constraints. In [25], an improved genetic algorithm was used to solve the problem of multi-objective cooperative trajectories planning for multi-parafoil systems. However, the two research works mainly focus on the trajectory planning of multi-parafoil systems, not involving trajectory tracking. Kaminer *et al.* [18] proposed a solution to the problem of a coordinated drop of multiple parafoils under strict spatial constraints. Firstly, feasible trajectories for every parafoil are generated in the planning space. Secondly, each parafoil is required to strictly execute a pure trajectory following maneuvers to ensure that no collision occurs between parafoils. Chen *et al.* [26] used the potential field method to study the rendezvous control of multiple parafoils. The designed algorithm can realize rendezvous control of multiple parafoils. Chen *et al.* [27] proposed the guidance algorithm for multi-parafoil systems based on virtual structure to achieve the coordinated airdrop. Calise *et al.* [17] studied the swarming or flocking and collision avoidance behavior for a mass airdrop of multiple autonomous parafoils. The feasibility of the concept was verified by simulations, and 5 parafoils were tested for cooperative control flight. Gurfil *et al.* [28] proposed a top-down approach for designing and executing airdrop missions

using multiple guided parafoils. The developed guidance algorithm and cooperative task management method can deal with faults and exceptional events for a parafoil group. Rosich *et al.* [29] proposed a new trajectory generation algorithm and developed behavior-based rules that control the relative motion of multiple descending parafoils. The behavior rules include cohesion, separation, and alignment. By adjusting the relative motion between parafoils, multiple parafoils could land at the same target and safe separation between the parafoils could be ensured. Note that [29] does not involve the formation problem of multi-parafoil systems.

We found from the related work that the mainstream methods to achieve a multi-parafoil cooperative airdrop are based on centralized control. They employ a control center to plan trajectories for every parafoil. Then each parafoil must strictly tracks the planned trajectory to achieve a multi-parafoil cooperative landing. However, the parafoil in this way usually lacks autonomy and flexibility. For example, once a parafoil fails to follow the trajectory or encounters a breakdown, the parafoil could be unable to recover autonomously, and may even need task reconfiguration. The control center must re-plan new trajectories for all parafoils, which would result in a significant increase in mission complexity. Meanwhile, because the flight time of a parafoil in the air is limited, the parafoil group may have landed on the ground before it can track the re-planned trajectory. However, in a distributed multi-parafoil systems, each parafoil has certain autonomous ability, so the parafoils working in this mode are more flexible.

III. The Preliminaries

The formation guidance for multi-parafoils systems could be realized by local information exchange between parafoils, which is based on graph theory. The following is a brief introduction for the fundamentals of graph theory.

Graph $\mathscr{G}$ can be represented by vertex sets $\mathscr{V}(\mathscr{G}) = \{v_i, ..., v_n\}$ and edge sets $\mathscr{E}(\mathscr{G}) \subset \mathscr{V} \times \mathscr{V}$, in which v_i is the vertex of the graph and $\{v_i, v_j\} \in \mathscr{E}(\mathscr{G})$ is the edge of the graph. The adjacency matrix $\boldsymbol{A} = [a_{ij}]_{N\times N}$ is a non-negative weighted matrix, which is used to describe the topological connection of a graph. The values of the non-negative elements a_{ij} correspond to the edges of the graph. Since there are no self-loop in the graph, so a_{ii} is 0. The matrix $\boldsymbol{D} = diag(d_1, d_2, \cdots, d_N)$ is diagonal, and each diagonal element corresponds to $d_i = \sum_{j\neq i} a_{ij}$. The Laplacian matrix of a graph is defined as $\boldsymbol{L} = \boldsymbol{D} - \boldsymbol{A}$. The set of all adjacent parafoils in the communication range of the i^{th} parafoil is called the neighbour set of the i^{th} parafoil, recorded as $\mathscr{N}_i = \{j \in \mathscr{V} \,|\, \{v_j, v_i\} \in \mathscr{E}\}$. The network topology of the multi-parafoils studied in this paper is based on the assumption that the multi-parafoils form a balanced and static communication network, and maintain a strong connection.

IV. The Algorithms

A. The Algorithm Overview

This paper provides a solution for the problem of the airdrop for massive goods and materials using multiple parafoils. We develop a coordinated airdrops framework that includes a leader-follower consensus-based formation guidance strategy with a trajectory planning and tracking algorithms. Fig. 2 depicts the overview of the framework. Firstly, the trajectory planning algorithm generates the multiphase homing trajectory for the pilot parafoil. Then, the pilot parafoil tracks the desired trajectory according to the trajectory tracking algorithm. Finally, the follower parafoils exchange the local state information with each other through the information flow topology to form the desired formation and maintain the desired safe distances, and reach the landing points.

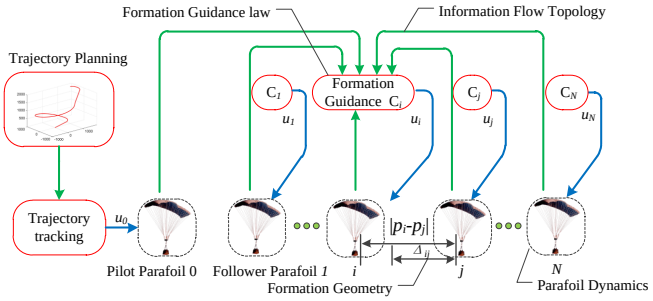

Fig. 2: The framework of multi-parafoil systems to achieve coordinated airdrops. The framework includes several parts: the parafoil dynamics describe the motion characteristic of the parafoil; the information flow topology defines the communication topology between the parafoils; the formation guidance law implements the distributed control only using the local neighbour information; the formation geometry ensures a safe distance between neighbouring parafoils.

B. The Multi-parafoil Systems Model

This paper mainly focuses on the motion control of the mass center of the parafoil system. Therefore, the particle model is used to establish the multi-parafoil systems model. Fig. 3 shows the force analysis diagram of the system.

The multi-parafoil systems consist of one pilot parafoil and N follower parafoils. From the force diagram, the particle model of each parafoil can be described by the following differential equations [17]:

$$\begin{cases} \dot{V}_i = -\frac{D_i + W_i \sin\gamma_i}{m_i} \\ \dot{\gamma}_i = \frac{L_i \cos\sigma_i - W_i \cos\gamma_i}{mV_i} \\ \dot{\varphi}_i = \frac{L_i \sin\sigma_i}{m_i V_i \cos\gamma_i} \end{cases}, \tag{1}$$

$$\begin{cases} \dot{x}_i = V_i \cos\gamma_i \cos\varphi_i + w_x \\ \dot{y}_i = V_i \cos\gamma_i \sin\varphi_i + w_y \\ \dot{z}_i = V_i \sin\gamma_i \end{cases}, \tag{2}$$

where $i = 0, 1, 2, \cdots, N$, $i = 0$ is regarded as the pilot parafoil, and the other parafoils are the followers. Taking the derivative of (2) with respect to time, and substituting (1) into the derivative of (2), the parafoil particle model can be converted into a quadratic integral model [30]:

$$\begin{cases} \dot{\boldsymbol{p}}_i = \boldsymbol{v}_i \\ \dot{\boldsymbol{v}}_i = \boldsymbol{u}_i \end{cases}, \tag{3}$$

where $\boldsymbol{p}_i = [x_i, y_i, z_i]^T \in \Re^3$ is the parafoil inertial position vector, $\boldsymbol{v}_i$ is the velocity vector and $\boldsymbol{u}_i = [u_{x_i}, u_{y_i}, u_{z_i}]^T \in \Re^3$ is the equivalent control input of the parafoil.

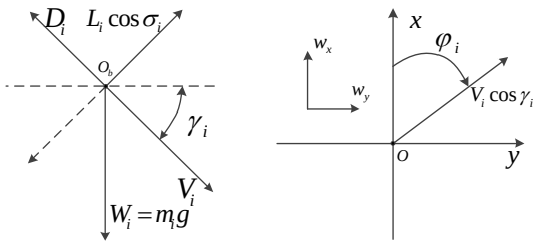

(a) Side view (b) Top view

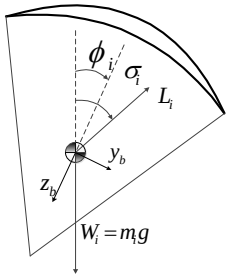

(c) Rear view

Fig. 3: Force analysis diagram of a parafoil system. L_i is lift force, and σ_i is the bank angle of lift force L_i. D_i is the aerodynamic drag force, which opposites to the velocity V_i. W_i is the gravity. γ_i is the glide angle. φ_i is the heading angle, w_x and w_y is the horizontal component of the wind speed in the x axis and y axis, respectively.

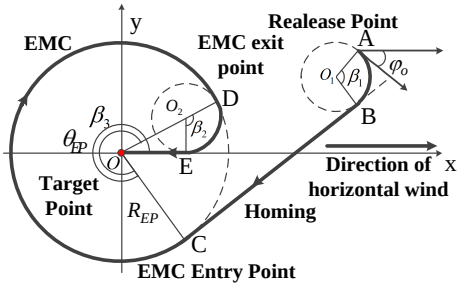

Fig. 4: The schematic diagram of multiphase homing trajectory for the parafoil. The homing trajectory is divided into three phases: the centripetal homing phase is from parafoil release point A to entry point C; the energy management control (EMC) phase is the great circle arc section, which starts from point C and ends at point D; the landing phase is from exit point D to target point O. Without loss of generality, we assume that the direction of the wind is consistent with the positive direction of the x-axis. If the parafoil approaches in the opposite direction to the wind, the parafoil can land upwind at the target point.

C. The Trajectory Planning Algorithm

In this paper, the leader-follower method is used to achieve cooperative formation airdrop. Taking the pilot parafoil as the leader, we need to plan its homing trajectory first.

At present, the commonly used parafoil trajectory planning algorithms can be roughly divided into the simple homing method [31], optimal homing method [32]–[34] and multiphase homing method. The simple homing method mainly includes radial homing and conical homing. The optimal homing method converts multiple optimization objectives into a single optimization objective function by weighting factors and then solves the problem by indirect or direct methods.

Multiphase trajectory planning is a relatively mature trajectory planning algorithm, which was adopted by NASA in its X-38 project [35]. The trajectory is generally divided into the centripetal homing phase, the energy management control (EMC) phase and the upwind landing phase.

Its control operation is simpler than optimal homing. Therefore, from the point of view of engineering practicability, this paper uses the multiphase homing trajectory for parafoil. The horizontal projection diagram is shown in Fig. 4.

In the multiphase homing method, the transition point from the centripetal homing phase to the energy management control (EMC) phase is generally called the entry point (EP). The parameter of the entry point C is (R_{EP}, θ_{EP}), where R_{EP} is the turning radius of the EMC phase, and θ_{EP} is the arc angle of enter point C. The parameters of the entry point are the keys to multiphase homing. The design objective is that the distance between planned target point and actual landing point should be minimum, and the turning radius R_{EP} should be within the parafoil performance range. The objective function is shown in (4):

$$\begin{aligned} J = {} & R_{\min}(\beta_1 + \beta_2) + (\|BC\| + \|EO\|) \\ & + (R_{EP}\beta_3 + 2\pi R_{EP}\tau) - z_0 / |\tan\gamma|, \end{aligned} \tag{4}$$

where $R_{\min}$ is the minimum turning radius of the parafoil shown in Fig. 4, β_1 and β_2 are the angles of the transition phase, β_3 is the turning angles of the EMC phase, and $\|BC\|$ and $\|EO\|$ is the length of the centripetal homing phase and the upwind landing phase, respectively. γ is the glide angle of the parafoil, and τ is the number of spiralling circles at higher altitudes. For a detailed introduction to this objective function, please refer to the papers [7] and [34].

The pseudo-code of the trajectory planning algorithm proposed in this paper is shown in algorithm 1. The general idea of the algorithm is that the radius and arc angle of the entry point C are taken as chromosomes to generate homing trajectory according to the geometric relationship shown in Fig. 4. Every time a trajectory is generated, one iteration is completed. Then, the survival of the fittest principle is used to generate the entry point of the next generation [36], so that the landing point of the generated trajectory is closer and closer to the target point, and finally the optimal trajectory is obtained.

D. The Trajectory Tracking Algorithm

It is the first step to plan a feasible flight trajectory for the pilot parafoil, but it is more important for the pilot parafoil to track the planned trajectory so as to achieve precise airdrop. Firstly, the deviation between the current position of the parafoil and the planned reference position is calculated. Then, the control variables are calculated by using

Algorithm 1: Trajectory planning algorithm

Input: parafoil initial state $(x_0, y_0, z_0, \varphi_0)$, glide angle γ_0, minimum turning radius $R_{\min}$, target point state $(0,0,0,\pi)$, etc.

Output: the generated reference trajectory

set the parameter (R_{EP}, θ_{EP}) range;
set genetic algorithm parameter(population size, generations, etc.);
$i \leftarrow 0$;
$Pop_0 \leftarrow$intial population(population size, etc.);
Evaluate_fitness(Pop_0) using (4);
while *termination condition does not hold* **do**
    $i \leftarrow i+1$;
    selection Pop_i from Pop_{i-1};
    crossover(Pop_i);
    mutation(Pop_i);
    Evaluate_fitness(Pop_i) using (4);
    update population
end
get the optimal solution;
generate multiphase homing trajectory;

an appropriate control algorithm to adjust the parafoil flight states and eliminate the deviations. This paper combines the lateral offset and the heading angle errors to produce control instructions. Fig. 5 shows the trajectory tracking schematic diagram in the horizontal plane.

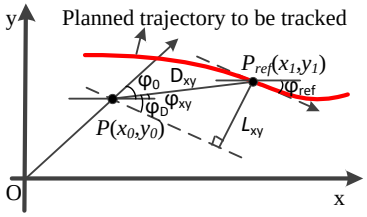

Fig. 5: Schematic diagram of horizontal trajectory tracking based on position and heading angle error. The red line represents the planned trajectory, P_{ref} represents the reference point on the planned trajectory, and P represents the current position of the parafoil.

In Fig. 5, the D_{xy} represents the distance between the reference point and the current position of the parafoil, which is defined as:

$$D_{xy} = \sqrt{(x_1 - x_0)^2 + (y_1 - y_0)^2}. \tag{5}$$

The angle between D_{xy} and x-axis is defined as φ_{xy}, which can be obtained through $\varphi_{xy} = \arctan\left((y_1 - y_0)/(x_1 - x_0)\right)$. If the heading angle of the parafoil is φ_0, the reference heading angle is φ_{ref}, then the heading angle error φ_{error} is:

$$\varphi_{error} = \varphi_{ref} - \varphi_0. \tag{6}$$

When calculating the heading angle error, the following formulas are employed to limit the error to the range $[-\pi, \pi]$:

$$\varphi_{error} = \varphi_{ref} - \varphi_0, \begin{cases} \varphi_{error} = \varphi_{error} - 2\pi, \varphi_{error} \geq \pi \\ \varphi_{error} = \varphi_{error}, -\pi < \varphi_{error} < \pi \\ \varphi_{error} = \varphi_{error} + 2\pi, \varphi_{error} \leq -\pi \end{cases}. \tag{7}$$

The lateral offset L_{xy} between the current position of the parafoil and the planned point is defined as follows:

$$L_{xy} = D_{xy} \cdot \sin\varphi_D = D_{xy} \cdot \sin(\varphi_{ref} + \varphi_{xy}), \tag{8}$$

where, φ_D is the angle between D_{xy} and the reference point tangent.

Based on the lateral offset and heading angle error, the following horizontal tracking controller is designed in this paper:

$$u_1 = \dot{\varphi}_0 = k_1 \cdot L_{xy} + k_2 \cdot \varphi_{error}, u_1 \in [-u_{1\max}, u_{1\max}], \tag{9}$$

where u_1 is the turning angle rate of the parafoil. By choosing the appropriate coefficient k_1 and k_2, the parafoil can track the reference trajectory on the horizontal plane. In addition, the asymmetric pull-down of the parafoil is limited, so the turning angle rate of the parafoil is limited. Therefore, the above control variables must be saturated to satisfy the constraints of the turning angle rate.

Currently, parafoil trajectory tracking mainly adjusts directions according to the errors in the horizontal plane. In such a case, the parafoil descent velocity and glide angle are assumed to be constant. But in fact, within a certain range, the descent velocity and glide angle can also be controlled in the longitudinal plane by symmetrical pull-down of the parafoil control rope. The parafoil can superimpose the asymmetrical pull-down on the symmetrical pull-down to realize horizontal and longitudinal control simultaneously.

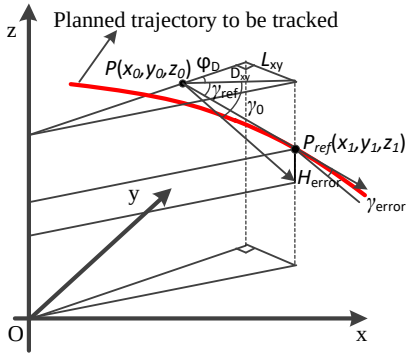

Fig. 6: Schematic diagram of longitudinal trajectory tracking based on the vertical position and glide angle error. γ_0 is the glide angle of the pilot parafoil and γ_{ref} is the reference glide angle at the point P_{ref} of the reference trajectory.

In Fig. 6, the error of the glide angle γ_{error} is:

$$\gamma_{error} = \gamma_{ref} - \gamma_0. \tag{10}$$

Similar to the heading angle error, the glide angle error also needs to be limited:

$$\gamma_{error} = \gamma_{ref} - \gamma_0, \begin{cases} \gamma_{error} = \gamma_{error} - 2\pi, \gamma_{error} \geq \pi \\ \gamma_{error} = \gamma_{error}, -\pi < \gamma_{error} < \pi \\ \gamma_{error} = \gamma_{error} + 2\pi, \gamma_{error} \leq -\pi \end{cases}. \tag{11}$$

The height error H_{error} is:

$$H_{error} = D_{xy} \cdot \tan\left(\gamma_{ref}\right) - D_{xy} \cdot \tan\left(\gamma_0\right). \tag{12}$$

Similar to the horizontal tracking control, the longitudinal tracking controller is designed as follows:

$$u_2 = \dot{\gamma}_0 = k_3 \cdot H_{error} + k_4 \cdot \gamma_{error}, u_2 \in [u_{2\min}, u_{2\max}]. \quad (13)$$

Among them, u_2 is the parafoil glide angle rate. Because the symmetrical pull-down quantity of the control rope of the parafoil is limited, the longitudinal tracking controller also should be saturated to limit the control quantity. In this paper, the range of the parafoil glide angle is chosen to be $[-8°, -16°]$. The trajectory tracking algorithm is shown in algorithm 2. The algorithm firstly calculates the position

Algorithm 2: Trajectory Tracking algorithm

Input: parafoil reference trajectory point (x_1, y_1, z_1), parafoil current state (x_0, y_0, z_0), etc.
Output: the control quantity and endflag

$Num \leftarrow$Total number of trajectory reference point;
if $i < Num$ **then**
  calculate D_{xy}, φ_{xy}, φ_D, L_{xy} and φ_{error}; limit φ_{error} to $-\pi$ and π using (7);
  obtain lateral control quantity $u_1 = k_1 \cdot L_{xy} + k_2 \cdot \varphi_{error}$;
  calculate $D_{xyz} = \sqrt{(x_1 - x_0)^2 + (y_1 - y_0)^2 + (z_1 - z_0)^2}$;
  calculate H_{error}, γ_{error} and $\gamma_{ref} = asin\left(((z_1 - z_0))/D_{xyz}\right)$;
  limit γ_{error} to $-\pi$ and π using (11);
  obtain longitudinal control quantity $u_2 = k_3 \cdot H_{error} + k_4 \cdot \gamma_{error}$;
  if $\varphi_D > \frac{\pi}{2} || L_{xy} < 1$ **then**
    $i \leftarrow i + 1$;
    endflag $\leftarrow 0$;
  end
else
  endflag $\leftarrow 1$;
end

and angle error between the current point of the parafoil and reference point in the horizontal and longitudinal plane. Then, by adjusting the parafoil flight direction to minimize the errors and the parafoil system move to the reference point. When the lateral offset L_{xy} is less than 1, or angle φ_D is greater than $\pi/2$, the algorithm switches to the next reference point. If it switches to the final reference point, the parafoil system achieves a precise landing.

E. The Formation Guidance Algorithm for Multi-Parafoil Systems

Formation guidance refers to the problem that multiple agents can not only maintain a certain geometry (or formation) but also avoid collision when moving towards moving towards a specific destination or direction. The aim of formation control is to synchronize the position and speed of multi-parafoils, and each parafoil flies steadily by a required formation.

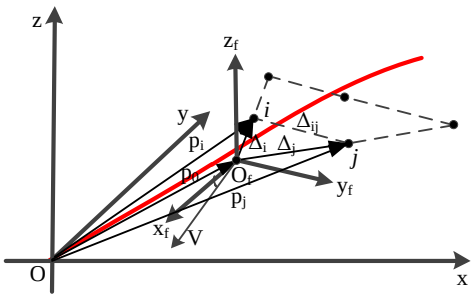

Fig. 7: Schematic diagram of a parafoil coordinate system. Point O_f is the current position of the pilot parafoil, which may deviate from the planned trajectory represented by the red line.

As shown in Fig. 7, there are two coordinate systems: one is the inertial coordinate system $Oxyz$; the other one is the formation coordinate system $O_f x_f y_f z_f$. The current position of the pilot parafoil in the inertial coordinate system is defined as the origin of the formation coordinate system. In the formation coordinate system, the distance vectors of the follower parafoil relative to the pilot parafoil are expressed by Δ_i and Δ_j. Δ_{ij} is the distance between parafoil i and j. $\boldsymbol{p}_0$, $\boldsymbol{p}_i$ and $\boldsymbol{p}_j$ is the inertia position of the pilot parafoil, and the follower parafoil i and follower parafoil j, respectively. Then, there exist $\boldsymbol{p}_i = \boldsymbol{p}_0 + \Delta_i$, $\boldsymbol{p}_j = \boldsymbol{p}_0 + \Delta_j$, $\Delta_{ij} = \boldsymbol{p}_i - \boldsymbol{p}_j = \Delta_i - \Delta_j$. The desired formation configuration can be defined by a set of position coordinates $\Delta_f = [\ \Delta_1^T \quad \Delta_2^T \quad \cdots \quad \Delta_N^T\ ]^T$ in the formation coordinate system.

In this paper, the communication network topology is fixed in the formation process. The topology diagram is shown in Fig. 8, in which p_0 is the pilot parafoil and the others are the follower parafoils.

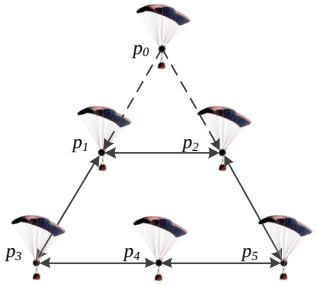

Fig. 8: Topology of a multi-parafoil systems. Pilot parafoil p_0 transmits information to some follower parafoil, and the local information is exchanged between the follower parafoil. The topology graph is undirected.

1) Cooperative Formation Guidance Algorithm for Multi-parafoil Systems: In order to realize the cooperative formation airdrop of multi-parafoil systems, the guidance law is

designed in as (14),

$$\begin{aligned}\boldsymbol{u}_i(t) =& \boldsymbol{u}_{i-form}(t)+\boldsymbol{u}_{i-vel}(t), && (14)\\ \boldsymbol{u}_{i-form}(t) =& -\sum_{j\in\mathcal{N}_i}\boldsymbol{K}_1 a_{ij}\left(\boldsymbol{p}_i(t)-\boldsymbol{p}_j(t)-\Delta_{ij}\right)\\ & -\boldsymbol{K}_3 c_i\left(\boldsymbol{p}_i(t)-\boldsymbol{p}_0(t)-\Delta_i\right), && (15)\\ \boldsymbol{u}_{i-vel}(t) =& -\sum_{j\in\mathcal{N}_i}\boldsymbol{K}_2 a_{ij}\left(\boldsymbol{v}_i(t)-\boldsymbol{v}_j(t)\right)\\ & -\boldsymbol{K}_4 c_i\left(\boldsymbol{v}_i(t)-\boldsymbol{v}_0(t)\right), && (16)\end{aligned}$$

where $\boldsymbol{u}_{i-form}(t)$ is the formation control variables, $\boldsymbol{u}_{i-vel}(t)$ is the velocity consensus control variables, and $\boldsymbol{K}_1$, $\boldsymbol{K}_2$, $\boldsymbol{K}_3$, $\boldsymbol{K}_4 \in \mathbb{R}^{3\times 3}$ are positive definite matrices, $\boldsymbol{K}_1$ and $\boldsymbol{K}_2$ represents the proportion of the formation and the velocity consensus in the algorithm, respectively. $\boldsymbol{K}_3$ and $\boldsymbol{K}_4$ represents the proportion of the position error and the velocity error between the follower parafoil and the pilot parafoil, respectively. c_i represents the communication connection between follower parafoil i and the pilot parafoil. $c_i = 1$ indicates that the follower parafoil can receive the information from the pilot parafoil, while $c_i = 0$ means that there is no direct communication connection. $\boldsymbol{u}_i(t) = [u_{x_i}(t)u_{y_i}(t)u_{z_i}(t)]^T$ is the total equivalent control vector of the follower parafoil.

2) Stability Analysis of Multi-Parafoil Systems: Firstly, the formation error $E_1(t)$ of multi-parafoil systems is defined as

$$\begin{aligned}E_1(t) =& \tfrac{1}{2}\sum_{i=1}^{N}\sum_{j\in\mathcal{N}_i} a_{ij}\left[\boldsymbol{p}_i-\boldsymbol{p}_j-\Delta_{ij}\right]^T\boldsymbol{K}_1\left[\boldsymbol{p}_i-\boldsymbol{p}_j-\Delta_{ij}\right]\\ =& \tfrac{1}{2}\sum_{i=1}^{N}\sum_{j\in\mathcal{N}_i} a_{ij}\left[(\boldsymbol{p}_i-\boldsymbol{p}_0-\Delta_i)-(\boldsymbol{p}_j-\boldsymbol{p}_0-\Delta_j)\right]^T\times\cdots\\ & \boldsymbol{K}_1\left[(\boldsymbol{p}_i-\boldsymbol{p}_0-\Delta_i)-(\boldsymbol{p}_j-\boldsymbol{p}_0-\Delta_j)\right],\end{aligned} \tag{17}$$

then, the following error $E_2(t)$ between the follower parafoil position and the pilot parafoil position is defined as

$$E_2(t) = \sum_{i\in\mathcal{N}_0} c_i\left[\boldsymbol{p}_i-\boldsymbol{p}_0-\Delta_i\right]^T\boldsymbol{K}_3\left[\boldsymbol{p}_i-\boldsymbol{p}_0-\Delta_i\right], \tag{18}$$

where $\mathcal{N}_0$ refers to the the adjacent set of the pilot parafoil. The total error is defined as $E(t) = E_1(t)+E_2(t)$.

Lemma 1*: If $\boldsymbol{L}$ is an undirected graph Laplacian matrix and $\boldsymbol{K}$ is a semi-positive definite matrix, $\boldsymbol{p} = \begin{bmatrix}\boldsymbol{p}_1^T & \boldsymbol{p}_2^T & \cdots & \boldsymbol{p}_N^T\end{bmatrix}^T$, there is*

$$\frac{1}{2}\sum_{i=1}^{N}\sum_{j\in\mathcal{N}_i} a_{ij}\left(\boldsymbol{p}_i-\boldsymbol{p}_j\right)^T\boldsymbol{K}\left(\boldsymbol{p}_i-\boldsymbol{p}_j\right) = \boldsymbol{p}^T(\boldsymbol{L}\otimes\boldsymbol{K})\boldsymbol{p}. \tag{19}$$

In (19) above, $\otimes$ is Kronecker's product.

Prove*:*

$$\begin{aligned}&\boldsymbol{p}^T(\boldsymbol{L}\otimes\boldsymbol{K})\boldsymbol{p}\\ =&\begin{bmatrix}\boldsymbol{p}_1^T l_{11}\boldsymbol{K}\boldsymbol{p}_1+\boldsymbol{p}_1^T l_{12}\boldsymbol{K}\boldsymbol{p}_2+\cdots+\boldsymbol{p}_1^T l_{1N}\boldsymbol{K}\boldsymbol{p}_N+\\ \boldsymbol{p}_2^T l_{21}\boldsymbol{K}\boldsymbol{p}_1+\boldsymbol{p}_2^T l_{22}\boldsymbol{K}\boldsymbol{p}_2+\cdots+\boldsymbol{p}_2^T l_{2N}\boldsymbol{K}\boldsymbol{p}_N+\\ \cdots\\ \boldsymbol{p}_N^T l_{N1}\boldsymbol{K}\boldsymbol{p}_1+\boldsymbol{p}_N^T l_{N2}\boldsymbol{K}\boldsymbol{p}_2+\cdots+\boldsymbol{p}_N^T l_{NN}\boldsymbol{K}\boldsymbol{p}_N\end{bmatrix}.\end{aligned}$$

As can be seen from the definition of Laplacian matrix elements $l_{ii} = \sum_{j\neq i}^{N} a_{ij}, i=j$; $l_{ij} = -a_{ij}$, $i \neq j$, the formula above can be rewritten as follows:

$$\begin{aligned}&\boldsymbol{p}^T(\boldsymbol{L}\otimes\boldsymbol{K})\boldsymbol{p}\\ =&\begin{bmatrix}\boldsymbol{p}_1^T\boldsymbol{K}\boldsymbol{p}_1\sum_{j\neq 1}^{N} a_{1j}-\boldsymbol{p}_1^T a_{12}\boldsymbol{K}\boldsymbol{p}_2-\cdots-\boldsymbol{p}_1^T a_{1N}\boldsymbol{K}\boldsymbol{p}_N\\ -\boldsymbol{p}_2^T a_{21}\boldsymbol{K}\boldsymbol{p}_1+\boldsymbol{p}_2^T\boldsymbol{K}\boldsymbol{p}_2\sum_{j\neq 2}^{N} a_{2j}-\cdots-\boldsymbol{p}_2^T a_{2N}\boldsymbol{K}\boldsymbol{p}_N\\ \cdots\\ -\boldsymbol{p}_N^T a_{N1}\boldsymbol{K}\boldsymbol{p}_1-\boldsymbol{p}_N^T a_{N2}\boldsymbol{K}\boldsymbol{p}_2-\cdots+\boldsymbol{p}_N^T\boldsymbol{K}\boldsymbol{p}_N\sum_{j\neq N}^{N} a_{Nj}\end{bmatrix}\\ =&\tfrac{1}{2}\sum_{i=1}^{N}\sum_{j\in\mathcal{N}_i} a_{ij}\left(\boldsymbol{p}_i-\boldsymbol{p}_j\right)^T\boldsymbol{K}\left(\boldsymbol{p}_i-\boldsymbol{p}_j\right).\end{aligned}$$

■

Let $\hat{\boldsymbol{p}} = [(\boldsymbol{p}_1-\boldsymbol{p}_0-\Delta_1)^T,\cdots,(\boldsymbol{p}_N-\boldsymbol{p}_0-\Delta_N)^T]^T$, by lemma 1, (17) can be written as $E_1(t) = \hat{\boldsymbol{p}}^T(\boldsymbol{L}\otimes\boldsymbol{K}_1)\hat{\boldsymbol{p}}$.

Define matrix $\boldsymbol{C} = diag[c_1, c_2, \cdots, c_N]$, and then Formula 18 can be written as:

$$\begin{aligned}&E_2(t) = \sum_{i\in\mathcal{N}_0} c_i\left[\boldsymbol{p}_i-\boldsymbol{p}_0-\Delta_i\right]^T\boldsymbol{K}_3\left[\boldsymbol{p}_i-\boldsymbol{p}_0-\Delta_i\right]\\ &=\sum_{i\in\mathcal{N}_0} c_i\hat{\boldsymbol{p}}_i^T\boldsymbol{K}_3\hat{\boldsymbol{p}}_i\\ &=\begin{bmatrix}\hat{\boldsymbol{p}}_1^T & \hat{\boldsymbol{p}}_2^T & \cdots & \hat{\boldsymbol{p}}_N^T\end{bmatrix}\begin{bmatrix}c_1\boldsymbol{K}_3 & 0 & \cdots & 0\\ 0 & c_2\boldsymbol{K}_3 & \cdots & 0\\ \vdots & \vdots & \ddots & \vdots\\ 0 & 0 & \cdots & c_N\boldsymbol{K}_3\end{bmatrix}\begin{bmatrix}\hat{\boldsymbol{p}}_1\\ \hat{\boldsymbol{p}}_2\\ \vdots\\ \hat{\boldsymbol{p}}_N\end{bmatrix}\\ &=\hat{\boldsymbol{p}}^T(\boldsymbol{C}\otimes\boldsymbol{K}_3)\hat{\boldsymbol{p}}.\end{aligned}$$

In summary, the error function can be written as $E(t) = \hat{\boldsymbol{p}}^T(\boldsymbol{L}\otimes\boldsymbol{K}_1+\boldsymbol{C}\otimes\boldsymbol{K}_3)\hat{\boldsymbol{p}}$.

The following Lyapunov function is constructed:

$$\begin{aligned}V =& \tfrac{1}{2}E+\tfrac{1}{2}\sum_{i=1}^{N}\dot{\hat{\boldsymbol{p}}}_i^T\dot{\hat{\boldsymbol{p}}}_i\\ =& \tfrac{1}{2}\hat{\boldsymbol{p}}^T(\boldsymbol{L}\otimes\boldsymbol{K}_1+\boldsymbol{C}\otimes\boldsymbol{K}_3)\hat{\boldsymbol{p}}+\tfrac{1}{2}\dot{\hat{\boldsymbol{p}}}^T\dot{\hat{\boldsymbol{p}}}.\end{aligned} \tag{20}$$

The derivative of the Lyapunov function can be obtained as follows:

$$\begin{aligned}\dot{V} =& \dot{\hat{\boldsymbol{p}}}^T(\boldsymbol{L}\otimes\boldsymbol{K}_1+\boldsymbol{C}\otimes\boldsymbol{K}_3)\hat{\boldsymbol{p}}+\dot{\hat{\boldsymbol{p}}}^T\ddot{\hat{\boldsymbol{p}}}\\ =& \dot{\hat{\boldsymbol{p}}}^T(\boldsymbol{L}\otimes\boldsymbol{K}_1+\boldsymbol{C}\otimes\boldsymbol{K}_3)\hat{\boldsymbol{p}}+\dot{\hat{\boldsymbol{p}}}^T\boldsymbol{u}\\ =& \dot{\hat{\boldsymbol{p}}}^T\left[(\boldsymbol{L}\otimes\boldsymbol{K}_1+\boldsymbol{C}\otimes\boldsymbol{K}_3)\hat{\boldsymbol{p}}+\boldsymbol{u}\right],\end{aligned} \tag{21}$$

where, $\boldsymbol{u} = \begin{bmatrix}\boldsymbol{u}_1^T & \boldsymbol{u}_2^T & \cdots & \boldsymbol{u}_N^T\end{bmatrix}^T$. In combination with lemma 1, the controller of (14) can be written as the following vector form:

$$\boldsymbol{u} = -[(\boldsymbol{L}\otimes\boldsymbol{K}_1+\boldsymbol{C}\otimes\boldsymbol{K}_3)]\hat{\boldsymbol{p}}-[(\boldsymbol{L}\otimes\boldsymbol{K}_2+\boldsymbol{C}\otimes\boldsymbol{K}_4)]\dot{\hat{\boldsymbol{p}}}. \tag{22}$$

By substituting (22) into (21), we can obtain

$$\dot{V} = -\dot{\hat{\boldsymbol{p}}}^T[(\boldsymbol{L}\otimes\boldsymbol{K}_2+\boldsymbol{C}\otimes\boldsymbol{K}_4)]\dot{\hat{\boldsymbol{p}}}. \tag{23}$$

It can be seen from (23), $\dot{V}$ is negative definite. According to Lyapunov theory, the error function $E(t)$ would approach zero. The follower parafoils can form stable formation and follow the pilot parafoil along the planned trajectory to the target point.

3) Collision Avoidance of Multi-Parafoil Systems: The above guidance strategy based on consensus achieves the formation control of the multi-parafoil systems, but it does not guarantee the collision avoidance when the parafoils turn abruptly. Therefore, the local collision avoidance term shown in (24) is designed based on the repulsive potential field method:

$$\begin{aligned} &\boldsymbol{u}_{i-avoid}(t) = -\boldsymbol{K}_5 \sum_{j\in\mathcal{N}_i} \frac{1}{e^{\left|\boldsymbol{p}_i(t)-\boldsymbol{p}_j(t)\right|/20}} \frac{\boldsymbol{p}_i(t)-\boldsymbol{p}_j(t)}{\left|\boldsymbol{p}_i(t)-\boldsymbol{p}_j(t)\right|}, \\ &\left|\boldsymbol{u}_{i-avoid}\right| \in [0, \boldsymbol{u}_{i-\max}], \end{aligned} \tag{24}$$

where $\left|\boldsymbol{p}_i(t)-\boldsymbol{p}_j(t)\right|$ is the spacing distance between parafoil i and parafoil j. When the distance is less than 20 m, the collision risk is large and the repulsive force will increase rapidly; on the contrary, when the distance is greater than 20 m, the repulsive force decreases rapidly. When the distance is about 50 m, the repulsive force almost decreases to 0, which does not affect the normal formation process. In order to limit the operating force of the parafoil, when increasing to a certain extent, the repulsive force will not increase after reaching the maximum saturation value. After considering the collision avoidance term, the overall guidance law is as follows:

$$\boldsymbol{u}_i(t) = \boldsymbol{u}_{i-form}(t) + \boldsymbol{u}_{i-vel}(t) + \boldsymbol{u}_{i-avoid}(t). \tag{25}$$

The pseudo-code of the cooperative formation algorithm for parafoil i is shown as Algorithm 3.

Algorithm 3: Formation Algorithm for Parafoil i

Input: pilot parafoil state, follower parafoil state, formation vector Δ_f, adjacency matrix $\boldsymbol{A}$, The total number N of parafoil, etc.

Output: the control quantity for follower parafoil i

Obtain the position $\boldsymbol{p}_0$, $\boldsymbol{p}_i$, $\boldsymbol{p}_j$ and speed $\boldsymbol{v}_0$, $\boldsymbol{v}_i$, $\boldsymbol{v}_j$ of the pilot parafoil and the follower parafoil;

Calculate the real formation coordinate Δ_{ij} by using formation vector Δ_f;

$\boldsymbol{u}_{i-form} \leftarrow 0, \boldsymbol{u}_{i-vel} \leftarrow 0, \boldsymbol{u}_{i-avoid} \leftarrow 0, \boldsymbol{u}_i \leftarrow 0$;

for j=1 *to* N **do**

  if $j \neq i$ **then**

    $\boldsymbol{u}_{i-form} \leftarrow \boldsymbol{u}_{i-form} - \boldsymbol{K}_1 a_{ij}\left(\boldsymbol{p}_i(t)-\boldsymbol{p}_j(t)-\Delta_{ij}\right)$;

    $\boldsymbol{u}_{i-vel} \leftarrow \boldsymbol{u}_{i-vel} - \boldsymbol{K}_2 a_{ij}\left(\boldsymbol{v}_i(t)-\boldsymbol{v}_j(t)\right)$;

    $\boldsymbol{u}_{i-avoid} \leftarrow \boldsymbol{u}_{i-avoid} - \boldsymbol{K}_5 \frac{1}{e^{\left|\boldsymbol{p}_i(t)-\boldsymbol{p}_j(t)\right|/20}} \frac{\boldsymbol{p}_i(t)-\boldsymbol{p}_j(t)}{\left|\boldsymbol{p}_i(t)-\boldsymbol{p}_j(t)\right|}$.

  end

end

$\boldsymbol{u}_i(t) \leftarrow \boldsymbol{u}_{i-form} + \boldsymbol{u}_{i-vel} + \boldsymbol{u}_{i-avoid} - \boldsymbol{K}_3 c_i\left(\boldsymbol{p}_i(t)-\boldsymbol{p}_0(t)-\Delta_i\right) - \boldsymbol{K}_4 c_i\left(\boldsymbol{v}_i(t)-\boldsymbol{v}_0(t)\right)$

V. Experimental Results and Discussions

In order to validate the effectiveness of the proposed algorithm, simulation experiments are carried out with MATLAB.

A. Trajectory Planning Results

Firstly, we perform simulations of the trajectory planning algorithm.The initial conditions and planned results are shown in Tab. I.

TABLE I: The initial conditions and the planned results.

Case No.	Initial coordinate	angle	Entry Point (R_{EP}, θ_{EP})
1	$(1500, 600, 2000)$	$45°$	$(1014.7, -86.1°)$
2	$(-1500, 600, 2000)$	$-45°$	$(1001.8, -55.1°)$

Without loss of generality, the initial glide angle γ_0 of the parafoil in all cases is set to 13°. In case 1, the optimal entry point parameters (R_{EP}, θ_{EP}) are found to be (1014.7, -86.1°). The distance between the planning landing point and the target point is 1.1×10^{-4} m, which meets the landing precision requirements. The initial condition of case 2 is different from that of case 1, but the algorithm in this paper can also effectively plan the accurate homing trajectory. The planned trajectories are shown in Fig. 9 and 10. It can be seen that the parafoil firstly adjusts its direction and makes a centripetal flight to the target, then consumes the height through the EMC phase and finally lands upwind to the target point. Fig. 11 shows the curves of the control quantities.

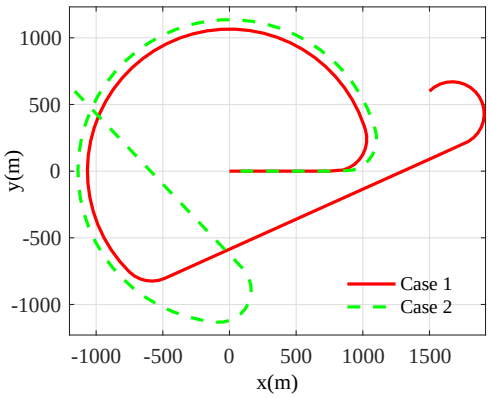

Fig. 9: 2-D view of the parafoil planned homing trajectory. The approaching direction of the parafoil is opposite to the wind direction (the wind direction is in the positive direction of the X-axis). The planned trajectories realize the upwind landing in both cases.

It can be seen that the parafoil is dominated by multiple constant control, this operation is relatively easy to realize in engineering.

B. Trajectory Tracking Results

Based on the planned trajectory, the trajectory tracking experiments are carried out with the controller designed by the position and angle error. The initial conditions are taken from case 1 in Tab. I. The actual initial release point is set to $(1600, 700, 1900)$. Thus, there is a position deviation between the actual release point and the planed initial point $(1500, 600, 2000)$. The characteristics parameters

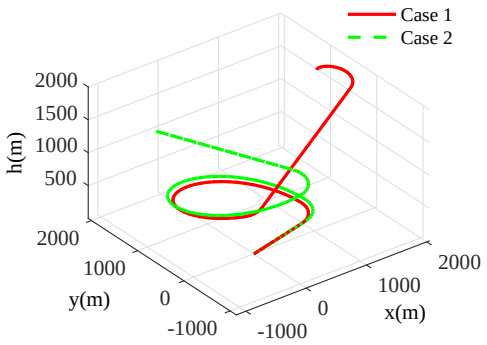

Fig. 10: 3-D view of the parafoil planned homing trajectory.

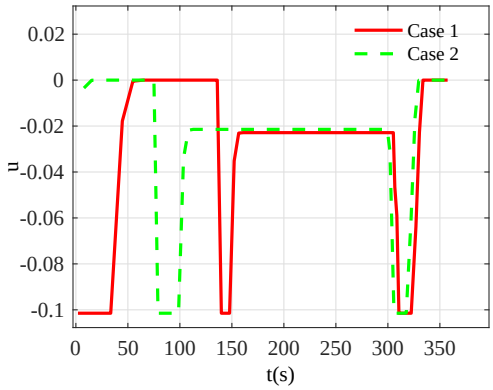

Fig. 11: Control quantity curve. It can be seen that the control quantities of the parafoil are nearly constant values, and the absolute values of the control quantities do not exceed the maximum allowable value, so the trajectories planned in this way are flyable.

of the parafoil and the coefficients k_1, k_2, k_3, k_4 of the controllers are shown in Tab. II.

In addition to the deviations of the initial positions, the disturbance of the random gust wind is also considered in this paper. As shown in Fig. 12, Gauss random gust wind with a mean of 0 m/s and covariance of 2 m/s is added between 50 s to 100 s.

The simulation result of the multiphase homing trajectory tracking in the horizontal plane is shown in Fig. 13. Fig. 14 shows the result in the 3-D space. It can be seen that even if the initial deviation is relative large, such as 100 m deviation in the three directions with gust wind disturbance, the parafoil was still gradually able to trace the planned trajectory. This demonstrates the disturbance rejection ability

TABLE II: Parameter settings for the simulations.

Parameters	Value/unit	Parameters	Value/unit
Initial glide angle	10°	Initial airdrop velocity	20 m/s
Horizontal speed V_s	$19.7m/s$	Vertical speed V_z	-3.5 m/s
Landing target	$(0,0,0)$	Minimum turn radius	105.6m
maximum turn rate	$0.178rad/s$	Upwind angle $\psi(t_f)$	180°
coefficients k_1	5/57.3	coefficients k_2	3
coefficients k_3	1/57.3	coefficients k_4	2

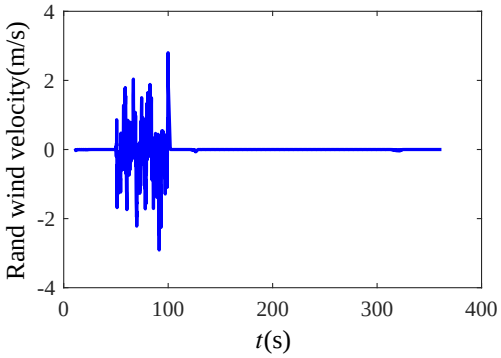

Fig. 12: Random gust wind disturbance.

of our tracking algorithm to the initial position deviations and gust wind disturbance.

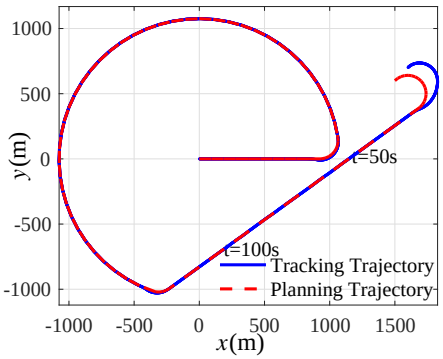

Fig. 13: Horizontal trajectory tracking effect.

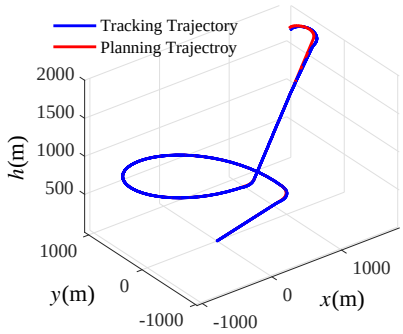

Fig. 14: 3-D trajectory tracking effect. After multiphase homing, the pilot parafoil finally lands upwind to the target point.

C. Formation Guidance Results

This section verifies the effectiveness of the formation guidance algorithm. We assume that 6 parafoils dropped at the same time, among which, one is the pilot parafoil and the others are the follower parafoils. The initial states and the final landing states of the parafoils under the guidance of formation algorithm are shown in Tab. III.

The designed formation is a triangular formation. The

TABLE III: The initial states and landing states.

Para.	Initial states		Landing states	
	coordinate	angle	coordinate	angle
0	(1600, 700, 1900)	45°	(−2.2, −2.5e − 8, 0.29)	180°
1	(2100, 800, 2000)	65°	(47.9, −50, 0.27)	−179.9°
2	(600, 1500, 2000)	80°	(47.8, 49.9, 0.28)	179.9°
3	(1800, 900, 2000)	75°	(97.8, −99.9, 0.27)	−179.9°
4	(500, 1900, 2000)	105°	(97.9, 0.0004, 0.27)	−179.9°
5	(800, 1300, 2000)	95°	(97.6, 100, 0.75)	179.9°

formation vector Δ_f in the formation coordinate system is

$$\Delta_f = \begin{bmatrix} -50 & 50 & 0 \\ -50 & -50 & 0 \\ -100 & 100 & 0 \\ -100 & 0 & 0 \\ -100 & -100 & 0 \end{bmatrix}. \tag{26}$$

According to the topological relationship shown in Fig. 8, the adjacency matrix $\boldsymbol{A} = [a_{ij}]_{N\times N}$ between the follower parafoils is defined as follows:

$$\boldsymbol{A} = \begin{bmatrix} 0 & 1 & 1 & 0 & 0 \\ 1 & 0 & 0 & 0 & 1 \\ 1 & 0 & 0 & 1 & 0 \\ 0 & 0 & 1 & 0 & 1 \\ 0 & 1 & 0 & 1 & 0 \end{bmatrix}. \tag{27}$$

Considering the physical constraints of the parafoils, the speed constraint of each parafoil is $18.8\,m/s \le V_i \le 32\,m/s$, the heading angle rate constraint of each parafoil is $\dot{\varphi}_i = \omega_i \le \omega_{\max}$=0.178 rad/s and the minimum turning radius of each parafoil is $r_{\min} = \frac{V_i}{\omega_{\max}}$=105.6 m. The data are taken from reference [29]. In addition, in the guidance law of Equation 25, $\boldsymbol{K}_1 = 0.2\boldsymbol{I}_3$, $\boldsymbol{K}_2 = 0.5\boldsymbol{I}_3$, $\boldsymbol{K}_3 = 0.1\boldsymbol{I}_3$, $\boldsymbol{K}_4 = 0.1\boldsymbol{I}_3$, $\boldsymbol{K}_5 = 100\boldsymbol{I}_3$. The simulation results of the formation guidance for the multi-parafoil system are shown in Fig. 15.

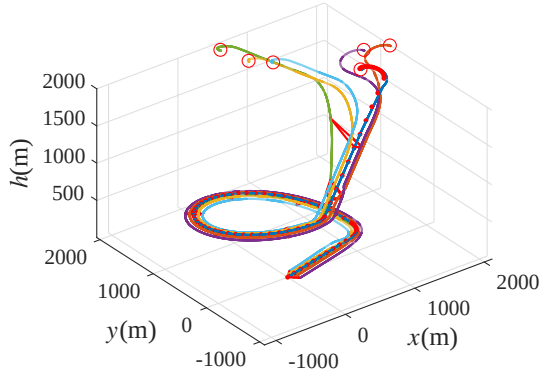

Fig. 15: The 3-D view of the formation flight trajectories of the multi-parafoil systems. The 6 circles represent the initial release points of the parafoils. The dotted red line represent the planned trajectory. It can be seen that the initial positions of the parafoils are scattered, but under the guidance of formation algorithm, the parafoils gradually gather close to each other.

Fig. 15 and Fig. 16 depict the trajectories of the multi-parafoil formation during airdrop. We can see that the

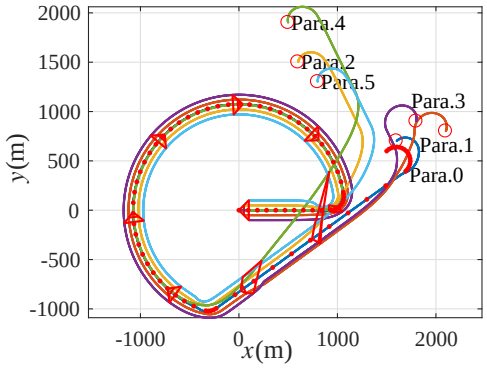

Fig. 16: The horizontal projection view of the flight trajectories of the multi-parafoil system. The triangle indicates the formation process of triangle formation. We can see that the parafoils gradually form the desired formation. Note that during the transition from the EMC phase to the landing phase, the formation shape changes, but returns to normal shape before landing.

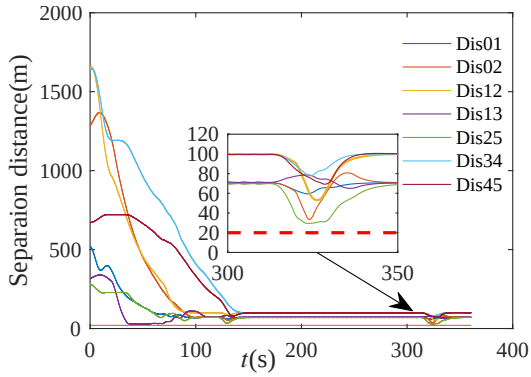

Fig. 17: The separation distance between parafoils. It can be seen that the minimum distance is greater than 20 m. The existence of collision avoidance term in the algorithm ensures that there is no collision during formation flight.

parafoils are dispersed at the beginning, and the initial heading angles are not the same as each other. However, under the guidance of the consensus formation algorithm, each parafoil gradually gathers together, instead of scattering apart. The coordinates of the final landing points of the six parafoils are shown in Tab. III. It can be seen that the dispersion of parafoils are small. Moreover, the desired triangular formation is formed gradually by the parafoils and is maintained during the airdrop process.

VI. Conclusion

The algorithms proposed here constitute the formation guidance strategy towards the cooperative airdrop of massive goods and materials using distributed multi-parafoil systems. Firstly, we proposed a trajectory planning algorithm for the pilot parafoil, with the consideration of two cases. Secondly, we developed a trajectory tracking algorithm, which includes both the lateral and longitudinal tracking control for the pilot parafoil. Finally, based on the planning and tracking algorithms, we designed a formation guidance strategy for

multi-parafoil systems. The experimental results show that all the parafoils could correctly form the desired formation without collision, and land at the desired point upwind.

However, there are some limitations in our work. Firstly, parafoils may encounter obstacles, such as mountains, buildings and forests, during a flight process, which have not been taken into consideration. Secondly, we only provided a solution for formation guidance. The altitude control for the parafoils was not involved. Finally, we performed the experiments only with simulations. The proposed strategy needs to be verified by real airdrop tests. Thus, in the future, we will integrate the obstacle avoidance and altitude control into the systems. Moreover, we will conduct real airdrop experiments with the proposed strategy.

REFERENCES

[1] Z. Zhang, Z. Zhao, and Y. Fu, "Dynamics analysis and simulation of six DOF parafoil system," *Cluster Computing*, pp. 1–12, 2018.

[2] L. Wang and W. He, "Analytical study on deformation and structural safety of parafoil," *International Journal of Aerospace Engineering*, vol. 2018, 2018.

[3] W. Tang and H. Johari, "Deformation of a ram-air canopy due to control line retraction," in *24th AIAA Aerodynamic Decelerator Systems Technology Conference*, 2017, p. 3546.

[4] J. Tao, W. Liang, Q. L. Sun, P. L. Tan, S. Z. Luo, Z. Q. Chen, and Y. P. He, "Modeling and control of a powered parafoil in wind and rain environments," *IEEE Transactions on Aerospace and Electronic Systems*, vol. 53, no. 4, pp. 1642–1659, 2017.

[5] M. Tanaka, K. Tanaka, and H. O. Wang, "Practical model construction and stable control of an unmanned aerial vehicle with a parafoil-type wing," *IEEE Transactions on Systems, Man, and Cybernetics: Systems*, pp. 1–7, 2018.

[6] Y. Ochi, "Modeling and simulation of flight dynamics of a relative-roll-type parafoil," in *Aiaa Scitech Forum*, 2020.

[7] H. Sun, Q. Sun, S. Luo, Z. Chen, W. Wu, J. Tao, and Y. He, "In-flight compound homing methodology of parafoil delivery systems under multiple constraints," *Aerospace Science and Technology*, vol. 79, pp. 85–104, 2018.

[8] M. J. Weinstein, B. J. Streetman, M. Neave, K. Bergeron, and G. Noetscher, "Trajectory optimization via particle swarms for robust parafoil guidance," in *2018 AIAA Guidance, Navigation, and Control Conference*, 2018, p. 1855.

[9] H. Sun, Q. Sun, Z. Chen, J. Tao, S. Luo, X. Zeng, X. Zeng, H. Teng, and P. Zhou, "An optimal-multiphase homing methodology for powered parafoil systems," *Optimal Control Applications and Methods*, pp. 1–25, 02 2020.

[10] P. Zhang, "Backstepping control based on L1 adaptive theory for large transport aircraft heavy load airdrop," *International Journal of Advanced Robotic Systems*, vol. 15, no. 1, pp. 1–10, 2018.

[11] H. Sun, Q. Sun, J. Tao, S. Luo, and Z. Chen, "A hybrid control approach for powered parafoil combining active disturbance rejection control and unbalanced load compensation," *Proceedings of the Institution of Mechanical Engineers, Part I: Journal of Systems and Control Engineering*, vol. 232, no. 3, pp. 299–314, 2018.

[12] M. R. Cacan and M. Costello, "Adaptive control of precision guided airdrop systems with highly uncertain dynamics," *Journal of Guidance, Control, and Dynamics*, vol. 41, no. 5, pp. 1025–1035, 2018.

[13] F. Binz, P. Hartmann, and D. Moormann, "Nonlinear model predictive flight path control for an unmanned powered paraglider," in *Advances in Aerospace Guidance, Navigation and Control*. Springer, 2018, pp. 369–387.

[14] E. Uhl, C. Schulte, C. Ulbrich, and O. Burkhardt, "FASTWing CL project: A self-navigated gliding system for capital loads," in *20th AIAA Aerodynamic Decelerator Systems Technology Conference and Seminar*, 2009, p. 2930.

[15] J. Stein, C. Madsen, and A. Strahan, "An overview of the guided parafoil system derived from X-38 experience," in *18th AIAA Aerodynamic Decelerator Systems Technology Conference and Seminar*, 2005, p. 1652.

[16] R. Benney, M. Henry, K. Lafond, A. Meloni, and S. Patel, "DoD new JPADS programs and NATO activities," in *20th AIAA Aerodynamic Decelerator Systems Technology Conference and Seminar*, 2009, p. 2952.

[17] A. J. Calise and D. Preston, "Swarming/flocking and collision avoidance for mass airdrop of autonomous guided parafoils," *Journal of guidance, control, and dynamics*, vol. 31, no. 4, pp. 1123–1132, 2008.

[18] I. Kaminer, O. Yakimenko, and A. Pascoal, "Coordinated payload delivery using high glide parafoil systems," in *18th AIAA aerodynamic decelerator systems technology conference and seminar*, 2005, p. 1622.

[19] L. Consolini, F. Morbidi, D. Prattichizzo, and M. Tosques, "Leader-follower formation control of nonholonomic mobile robots with input constraints," *Automatica*, vol. 44, no. 5, pp. 1343 – 1349, 2008. [Online]. Available: http://www.sciencedirect.com/science/article/pii/S0005109807004578

[20] Z. Peng, G. Wen, A. Rahmani, and Y. Yu, "Distributed consensus-based formation control for multiple nonholonomic mobile robots with a specified reference trajectory," *International Journal of Systems Science*, vol. 46, no. 8, pp. 1447–1457, 2015. [Online]. Available: https://doi.org/10.1080/00207721.2013.822609

[21] W. Lin, "Distributed UAV formation control using differential game approach," *Aerospaceence & Technology*, vol. 35, no. may, pp. 54–62.

[22] B. Das, B. Subudhi, and B. B. Pati, "Cooperative formation control of autonomous underwater vehicles: An overview," *International Journal of Automation & Computing*, vol. 13, no. 3, pp. 199–225.

[23] R. Rout and B. Subudhi, "A backstepping approach for the formation control of multiple autonomous underwater vehicles using a leaderâĂŞfollower strategy," *Journal of Marine Engineering & Technology*, vol. 15, no. 1, pp. 38–46, 2016.

[24] S. Luo, Q. Sun, J. Tao, W. Liang, and Z. Chen, "Trajectory planning and gathering for multiple parafoil systems based on pseudo-spectral method," in *2016 35th Chinese Control Conference (CCC)*. IEEE, 2016, pp. 2553–2558.

[25] C. Qi, Z. Min, J. Yanhua, and Y. Min, "Multi-objective cooperative paths planning for multiple parafoils system using a genetic algorithm," *Journal of Aerospace Technology and Management*, vol. 11, 2019.

[26] C. Qi, Z. Min, Z. Zhihao, M. Ma, and R. Huang, "Multiple autonomous parafoils system modeling and rendezvous control," *Acta Aeronautica et Astronautica Sinica*, vol. 37, no. 10, pp. 3121–3130, 2016.

[27] Q. Chen, Y. Sun, M. Zhao, and M. Liu, "A virtual structure formation guidance strategy for multi-parafoil systems," *IEEE Access*, vol. PP, pp. 1–1, 08 2019.

[28] P. Gurfil, S. Feldman, and M. Feldman, "Coordination and communication of cooperative parafoils for humanitarian aid," *IEEE Transactions on Aerospace and Electronic Systems*, vol. 46, no. 4, pp. 1747–1761, 2010.

[29] A. Rosich and P. Gurfil, "Coupling in-flight trajectory planning and flocking for multiple autonomous parafoils," *Proceedings of the Institution of Mechanical Engineers, Part G: Journal of Aerospace Engineering*, vol. 226, no. 6, pp. 691–720, 2012.

[30] P. K. Menon, G. D. Sweriduk, and B. Sridhar, "Optimal strategies for free-flight air traffic conflict resolution," *Journal of Guidance, Control, and Dynamics*, vol. 22, no. 2, pp. 202–211, 1999.

[31] Y. LI and H. LIN, "Theoretical investigation of gliding parachute trajectory with deadband and non-proportional automatic homing control," in *11th Aerodynamic Decelerator Systems Technology Conference*, 1991, p. 834.

[32] J. Huachen, L. Haiyan, Z. Detang, and Y. Jin, "Design of the optimal homing trajectory of a parafoil system considering threat avoidance," pp. 955–962, 2016.

[33] L. Haiyan, R. Zhigang, X. Chao, and Y. Jin, "Optimal homing trajectory design for parafoil systems using sensitivity analysis approach," *Control Theory & Applications*, vol. 32, no. 8, pp. 1003–1011, 2015.

[34] X. Jing, Q. Zizeng, and W. Hongwu, "Optimal control of parafoil system homing," *Aerospace Control*, vol. 22, no. 6, pp. 32–36, 2004.

[35] U. Soppa, T. Goerlach, and A. J. Roenneke, "German contribution to the X-38 CRV demonstrator in the field of guidance, navigation and control (GNC)," *Acta Astronautica*, vol. 56, no. 8, pp. p.737–749, 2005.

[36] X. Jing, Q. Zizeng, and C. Wenke, "Optimal design in multiphase trajectory of parafoil system," *Spacecraft Recovery and Remote Sensing*, vol. 25, no. 3, pp. 11–16, 2004.